arXiv:hep-ph/0106198 v2   17 Aug 2001

Pair Production of Smuons and Selectrons Near Threshold in e^+e^- and e^-e^- Collisions
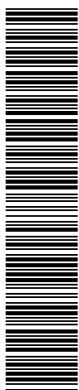
A. Freitas, D.J. Miller and P.M. Zerwas

Deutsches Elektronen–Synchrotron DESY, D–22603 Hamburg, Germany

Abstract

Non-zero width and Coulomb rescattering effects are analyzed for the pair production of smuons and selectrons near the thresholds in e^+e^- and e^-e^- collisions, respectively. The excitation curves are predicted in a gauge-invariant form. Energy cuts are designed to reduce irreducible supersymmetric backgrounds.

1   Introduction

In supersymmetric theories [1], scalar leptons are of particular interest. Their properties can be determined in $e^{\pm}e^-$ experiments with very high experimental precision [2, 3], which provides the platform for reconstructing the fundamental supersymmetric theory at energies up to near the Planck scale [4].

The supersymmetric partners of the left- and right-chiral leptons are the scalar leptons, $\tilde{l}_L$ and $\tilde{l}_R$. Neglecting mixing effects in the first and second family[1], the chiral states are identified with the mass eigenstates.

Scalar muons (likewise staus) are produced pairwise in e^+e^- annihilation via s-channel photon and Z boson exchange [5]:

$$e^+e^- \to \tilde{\mu}_i^+ \tilde{\mu}_i^- \quad (i = \mathrm{L/R}) \tag{1}$$

The cross-sections rise near the threshold $\sim \beta^3$ as a P-wave process $[\beta = (1 - 4m_{\tilde{\mu}_i}^2/s)^{\frac{1}{2}}$ denoting the smuon velocity], while becoming scale invariant for large centre-of-mass energies $\sqrt{s}$. In detail, the Born cross-sections for the production of on-shell smuons are given by

$$\sigma[e^+e^- \to \tilde{\mu}_i^+ \tilde{\mu}_i^-] = \frac{\pi\alpha^2}{3s}\,\beta^3 \Bigg[1 - g_i \frac{1 - 4s_W^2}{s_W c_W} \frac{s}{s - M_Z^2} + g_i^2 \frac{1 + (1 - 4s_W^2)^2}{16s_W^2 c_W^2} \left(\frac{s}{s - M_Z^2} \right)^2 \Bigg] \tag{2}$$

The masses are denoted by $m_{\tilde{\mu}_i}$ $(i = \mathrm{L/R})$ for the partners of the left- and right-chiral muon states; s_W and c_W are the sine and cosine of the electroweak mixing angle, and the couplings $g_L = (-1 + 2s_W^2)/4s_W c_W$ and $g_R = s_W/c_W$ denote the Z charges of the L/R smuons. The fine structure constant α is evaluated at the scale $\sqrt{s}$.

Scalar electrons, on the other hand, are in general produced by s-channel γ, Z and/or t-channel neutralino $\tilde{\chi}_j^0$ $(j = 1, ..., 4)$ exchanges [6]. In particular, for helicities L and R in e^+e^- and e^-e^- collisions, the mediating reactions and the types of orbital wave function near threshold are given by:

---

[1]Mixing effects in the smuon and selectron sectors are of the order 10^{-5} or less and can be safely neglected, provided the left- and right-chiral sleptons are well separated in mass.

$$e_L^+ e_R^- \,/\, e_R^+ e_L^- \quad \rightarrow \quad \tilde{e}_L^+ \tilde{e}_L^- , \tilde{e}_R^+ \tilde{e}_R^- \qquad [\gamma, Z;\, \tilde{\chi}^0] \qquad \text{P-wave} \qquad (3)$$

$$e_L^+ e_L^- \,/\, e_R^+ e_R^- \quad \rightarrow \quad \tilde{e}_R^+ \tilde{e}_R^- \,/\, \tilde{e}_L^+ \tilde{e}_L^- \qquad [\tilde{\chi}^0] \qquad\qquad \text{S-wave} \qquad (4)$$

$$e_L^- e_R^- \,/\, e_R^- e_L^- \quad \rightarrow \quad \tilde{e}_L^- \tilde{e}_R^- \qquad\qquad [\tilde{\chi}^0] \qquad\qquad \text{P-wave} \qquad (5)$$

$$e_L^- e_L^- \,/\, e_R^- e_R^- \quad \rightarrow \quad \tilde{e}_L^- \tilde{e}_L^- \,/\, \tilde{e}_R^- \tilde{e}_R^- \qquad [\tilde{\chi}^0] \qquad\qquad \text{S-wave} \qquad (6)$$

The steep rise $\propto \beta$ render S-wave production processes especially suitable for precision measurements in threshold scans. Left- and right-chiral selectrons can be generated in diagonal $\tilde{e}_L \tilde{e}_L$, $\tilde{e}_R \tilde{e}_R$ and mixed pairs $\tilde{e}_L \tilde{e}_R$. Since the amplitudes are built up solely by neutralino exchange, the total cross-sections for $e^- e^-$ collisions can be cast into a simple form:

$$\sigma[e_i^- e_i^- \rightarrow \tilde{e}_i^- \tilde{e}_i^-] = \frac{16\pi\alpha^2}{s} \sum_{j=1}^{4} \sum_{k=1}^{4} X_{ij}^2 \, X_{ik}^{*2} \, [G^{jk} + H^{jk}] \qquad (i = \text{L/R}) \qquad (7)$$

with

$$G^{jk} \;=\; \frac{2}{s} \frac{m_{\tilde{\chi}_j^0} m_{\tilde{\chi}_k^0}}{(\Delta_j + \Delta_k)} \left[\ln \frac{\Delta_j + \beta}{\Delta_j - \beta} + \ln \frac{\Delta_k + \beta}{\Delta_k - \beta} \right],$$

$$H^{jk} \;=\; \begin{cases} \dfrac{4\beta}{s} \dfrac{m_{\tilde{\chi}_j^0}^2}{\Delta_j^2 - \beta^2} & j = k \\[4mm] \dfrac{2}{s} \dfrac{m_{\tilde{\chi}_j^0} m_{\tilde{\chi}_k^0}}{(\Delta_j - \Delta_k)} \left[\ln \dfrac{\Delta_k + \beta}{\Delta_k - \beta} - \ln \dfrac{\Delta_j + \beta}{\Delta_j - \beta} \right] & j \neq k \end{cases} \qquad (8)$$

where $\Delta_j = 2(m_{\tilde{e}_i}^2 - m_{\tilde{\chi}_j^0}^2)/s - 1$ and $X_{ij} = (N'_{j1} - g_i N'_{j2})/\sqrt{2}$. The four neutralino masses in the minimal supersymmetric extension of the Standard Model (MSSM) are denoted by $m_{\tilde{\chi}_j^0}$ $(j = 1, ..., 4)$. The neutralino mixing matrix N' relates the mass eigenstates with the eigenstates in the photino-Zino-Higgsino basis.

For the mixed case in $e^+ e^-$ collisions:

$$\sigma[e_L^+ e_L^- \rightarrow \tilde{e}_R^+ \tilde{e}_L^-] = \frac{16\pi\alpha^2}{s} \sum_{j=1}^{4} \sum_{k=1}^{4} X_{Lj} \, X_{Rj}^* \, X_{Rk} \, X_{Lk}^* \; H^{jk} \qquad (9)$$

where the definitions of eq. (8) are understood, but with Δ_j replaced by $\overline{\Delta}_j = (m_{\tilde{e}_R}^2 + m_{\tilde{e}_L}^2 - 2m_{\tilde{\chi}_j^0}^2)/s - 1$ and $\beta = \sqrt{(s - m_{\tilde{e}_R}^2 - m_{\tilde{e}_L}^2)^2 - 4m_{\tilde{e}_R}^2 m_{\tilde{e}_L}^2}/s$. In contrast to the s-channel exchange process, these t-channel exchange cross-sections approach non-zero asymptotic values for high energies.

<u>Decays:</u> The right-chiral sleptons $\tilde{\mu}_R$ and $\tilde{e}_R$ decay predominantly into neutralinos while additional chargino decays are also important for left-chiral sleptons $\tilde{\mu}_L$ and $\tilde{e}_L$ [7]:

$$\Gamma(\tilde{l}_i^- \rightarrow l^- \tilde{\chi}_j^0) \quad = \quad \alpha |X_{ij}|^2 m_{\tilde{l}_i} \left(1 - \frac{m_{\tilde{\chi}_j^0}^2}{m_{\tilde{l}_i}^2} \right)^2 \qquad (i = L/R) \qquad (10)$$

$$\Gamma(\tilde{l}_L^- \rightarrow \nu_l \tilde{\chi}_k^-) \quad = \quad \frac{\alpha}{4} |U_{k1}|^2 m_{\tilde{l}_L} \left(1 - \frac{m_{\tilde{\chi}_k^-}^2}{m_{\tilde{l}_L}^2} \right)^2 \qquad (11)$$

While the notation for the neutralino sector has been defined above, $m_{\tilde{\chi}_k^\pm}$ $(k = 1, 2)$ denote the two chargino masses and U is the mixing matrix for the negative charginos. For a right-chiral slepton mass in the range of about 200 GeV, the widths are of the order $\Gamma_{\tilde{l}_R} \sim 700$ MeV, while left-chiral sleptons have widths of order 1 GeV.

2 Smuon Excitation

2.1 Threshold Behaviour

The measurement of the smuon excitation curve near the threshold is the most accurate method of determining their masses. Detailed simulations have demonstrated that the right-chiral smuon mass can be measured at TESLA to an accuracy of less than 100 MeV in this way [3], *i.e.* to a fraction of a per-mille. This experimental error is significantly smaller than the width of the state. Therefore, in this report we examine the effect of non-zero smuon widths on the excitation curves. Additionally, an accurate theoretical prediction requires the calculation of higher order effects, notably Coulomb rescattering among the final state particles. The problems arising in this context are quite similar to the production of W pairs in $e^+ e^-$ annihilations [8]. For the sake of clarity we will restrict ourselves to the analysis of right-chiral smuons[2].

Decays of the right-chiral smuons to the LSP $\tilde{\chi}_1^0$,

$$\tilde{\mu}_R^- \rightarrow \mu^- \tilde{\chi}_1^0 \qquad (12)$$

are by far the dominant decay mode in the MSSM. The parameters, masses and couplings, we have adopted for illustrative examples, correspond to the large $\tan \beta$ reference point

---

[2]Because of the low cross-section it is not possible to reach a precision for left-chiral smuons comparable to the case for right-chiral smuons.
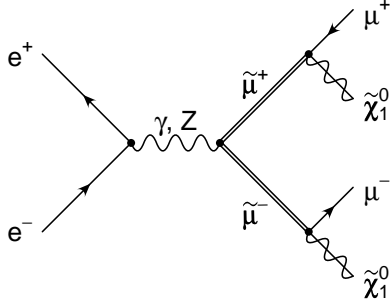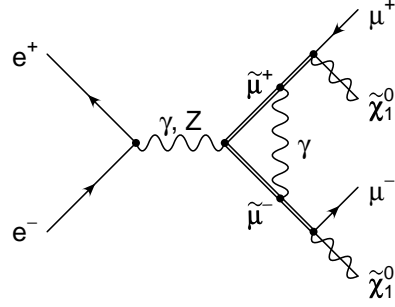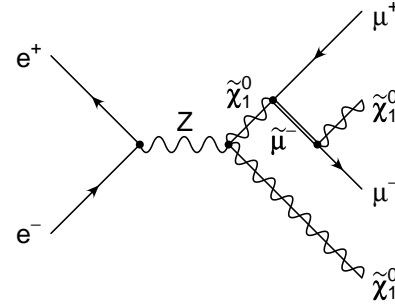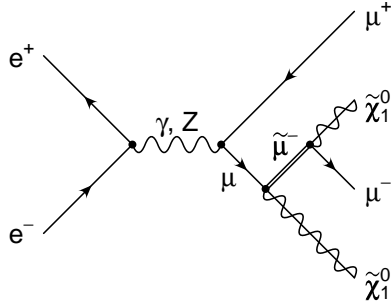
(a) <u>Double resonance diagram</u>   (c) <u>Coulomb rescattering</u>

(b) <u>Single resonance diagrams</u>

Figure 1: *The doubly (a) and singly (b) resonant smuon contributions to the process* $e^+e^- \to \mu^+\mu^- \tilde{\chi}_1^0 \tilde{\chi}_1^0$; *the Coulomb correction is described by diagram (c).*

RR2 in the TESLA study Ref. [9]. The relevant physical parameters are summarized in the appendix. The pair production of off-shell smuons is described in this final state by the diagram Fig. 1(a):

$$e^+e^- \to \mu^+\mu^- \tilde{\chi}_1^0 \tilde{\chi}_1^0 \tag{13}$$

However, the double resonance diagram must be supplemented by the single resonance diagrams of Fig. 1(b) to generate a gauge invariant set for the off-shell production amplitude.

If the $[\mu\tilde{\chi}_1^0]$ final states are studied near the $\tilde{\mu}$ mass, the real $\tilde{\mu}$ propagators must be replaced by the Breit-Wigner form which explicitly includes the non-zero width of the resonance state. Near the threshold the substitution leaves the set of diagrams Fig. 1 gauge invariant if the complex mass

$$m_{\tilde{\mu}}^2 \;\to\; M_{\tilde{\mu}}^2 = m_{\tilde{\mu}}^2 - i m_{\tilde{\mu}} \Gamma_{\tilde{\mu}} \tag{14}$$

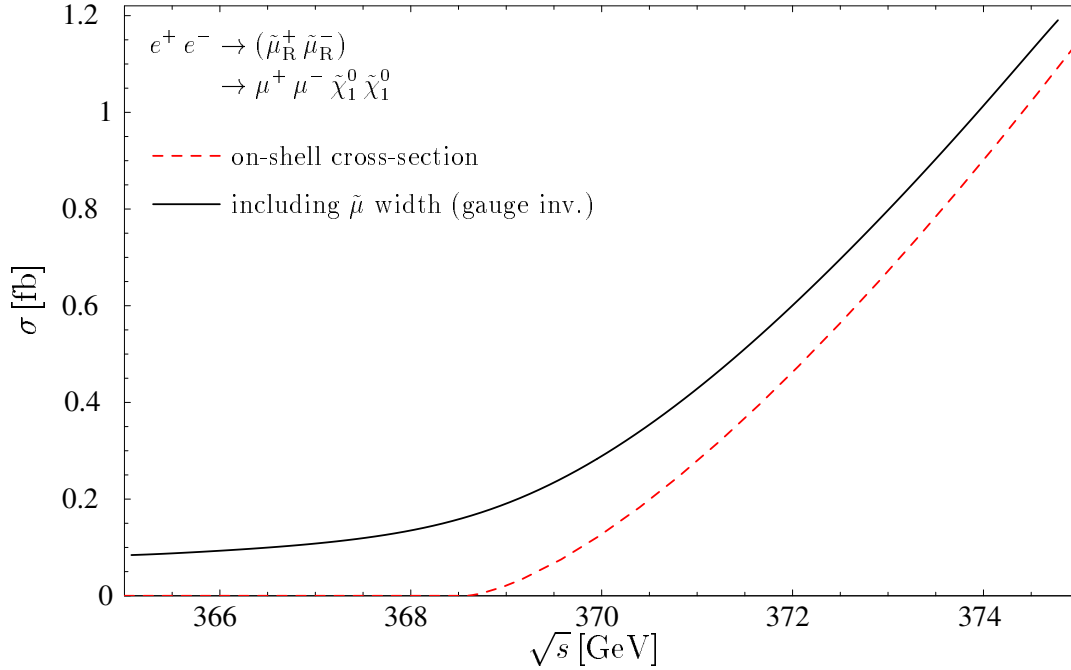is introduced with fixed width $\Gamma_{\tilde{\mu}}$. Applying the substitution to the propagators in the

Figure 2: *The effect of finite $\tilde{\mu}$ width on the $e^+e^- \to \tilde{\mu}_R^+\tilde{\mu}_R^- \to \mu^+\mu^-\tilde{\chi}_1^0\tilde{\chi}_1^0$ cross-section.*

double and single resonance amplitudes provides a consistent scheme for smuon production near the threshold. Even though taking only the doubly resonant contribution Fig. 1(a) with fixed width in the covariant gauge (a scheme generally adopted for experimental simulations [3]) is of sufficient accuracy at high energies, it fails for high-precision analyses near the threshold. Indeed the error induced by this method, about 80 MeV, is generally of the same size as the error of the experimental measurement.

The effect of non-zero width $\Gamma_{\tilde{\mu}_R}$ on the $\tilde{\mu}_R^+\tilde{\mu}_R^-$ excitation curve near the threshold is demonstrated in Fig. 2 for the *RR2* parameters. While the excitation curve is shown for zero width by the dotted line, the prediction of the excitation curve including the non-zero width effect in a gauge-invariant form is shown by the full line which can be interpreted as the "signal cross-section".

The Coulomb interaction due to the photon exchange, cf. Fig. 1(c), between slowly moving charged particles gives rise to large corrections of the threshold cross-section. Independent of spin and angular momentum, the threshold cross-section for stable particles is universally modified by $\sigma_{\text{Born}} \to (\alpha\pi/2\beta)\,\sigma_{\text{Born}}$ at leading order. This Sommerfeld rescattering correction [10] removes one power in the velocity β of the threshold sup-

pression $\sim \beta^{2l+1}$ for l-wave production. Multiple photon exchange further increases the cross-section but only by a very small amount.

However, for the production of off-shell particles the Coulomb singularity is partially screened [11]. Moreover, the correction depends on the orbital angular momentum l in this case[3]. For smuon P-wave production one finds at leading order

$$\sigma_{\text{Born}} \quad \rightarrow \quad \sigma_{\text{Born}} \frac{\alpha\pi}{2\beta_{\pm}} \left[1 - \frac{2}{\pi} \arctan \frac{|\beta_M|^2 - \beta_{\pm}^2}{2\beta_{\pm}\,\Im m\,\beta_M} \right] \Re e\,\mathcal{C}_1 \tag{15}$$

$$\mathcal{C}_l \quad = \quad \left[\frac{\beta_{\pm}^2 + \beta_M^2}{2\beta_{\pm}^2} \right]^l \tag{16}$$

with the generalized velocities

$$\beta_{\pm} \quad = \quad \lambda^{1/2}(s, m_+^2, m_-^2)/s \equiv \sqrt{(s - m_+^2 - m_-^2)^2 - 4m_+^2 m_-^2} \Big/ s \tag{17}$$

$$\beta_M \quad = \quad \sqrt{1 - 4M^2/s} \tag{18}$$

for the (complex) smuon pole mass M and the smuon virtualities m_+ and m_-. The off-shellness of the final state particles damps the Coulomb singularity. The damping for S-waves, described by the term in square brackets in eq. (15), is even stronger for waves of higher angular momentum l, due to the additional coefficient $\mathcal{C}_l$, as evident from Fig. 3. In contrast to W pair production, for larger energies $\sqrt{s} - 2m_{\tilde{\mu}} > \Gamma_{\tilde{\mu}}$ the off-shell Coulomb correction is slightly enhanced relative to the on-shell case, which is because the β^3 dependence of the production vertex distorts the integration over the Breit-Wigner resonances.

2.2 SUSY Backgrounds to SUSY Signals

The general Standard Model backgrounds contributing to the smuon signal in the process $e^+ e^- \rightarrow \mu^+ \mu^- + \not{\!E}$ are analyzed in Ref. [3]. Most significant are the production of W pairs with the leptonic decay $W \rightarrow \mu\nu$, and of γ/Z pairs with the decays $\gamma/Z \rightarrow \mu\mu$ and $\gamma/Z \rightarrow \nu\nu$. They can be reduced by observing that the decay leptons of the W's lie approximately in an azimuthal plane and the invariant mass of the lepton pair from γ/Z concentrate at the collinear and Z pole, respectively. The appropriate cuts and the detector acceptance allow a resulting signal efficiency of 50%.

---

[3]Since the production amplitude rises proportional to β^l near threshold, the maximum contribution is generated by the configuration of minimum orbital angular momentum l. For a general vertex $Y \rightarrow 2X$, l is the difference between $2j_X$ and j_Y for $2j_X < j_Y$, and 0/1 for even/odd j_Y otherwise.
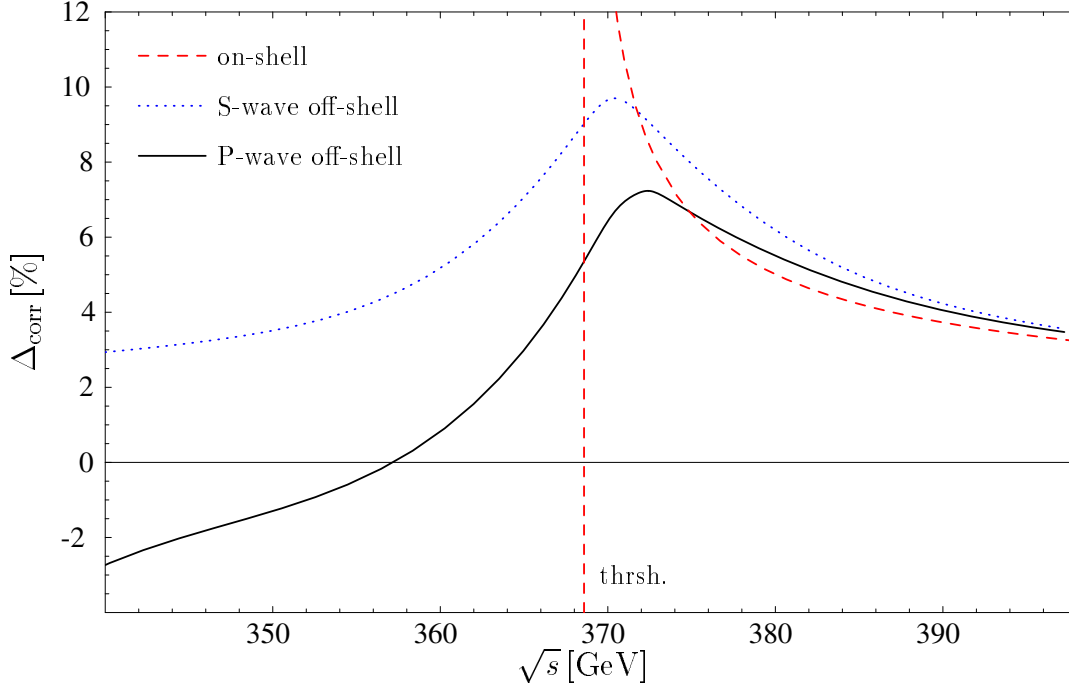
Figure 3: *Correction Δ_{corr} due to Coulomb rescattering effects relative to the Born cross-section for smuon production. The realistic case of off-shell P-wave production is compared with the correction factors for on-shell and off-shell S-wave production.*

Furthermore, a large number of SUSY backgrounds are involved, which had not been all included so far. Classes of background processes are catalogued in Tab. 1. The most important cross-sections are shown in Fig. 4(a). All these background processes can be reduced to a controllable level by applying cuts on the muon energies and on the missing energy. The SM motivated cuts of Ref. [3] have only little effect on the SUSY induced backgrounds and are not included in this analysis.

Background processes involve decay cascades which give rise to threshold effects in the muon-pair invariant mass and increased missing energy compared to the signal process. The large $\tilde{\chi}_2^0 \tilde{\chi}_1^0$ background can be reduced drastically by selecting events with invariant mass

$$m_{\mu\mu} \gtrsim m_{\tilde{\chi}_2^0} - m_{\tilde{\chi}_1^0} \tag{19}$$

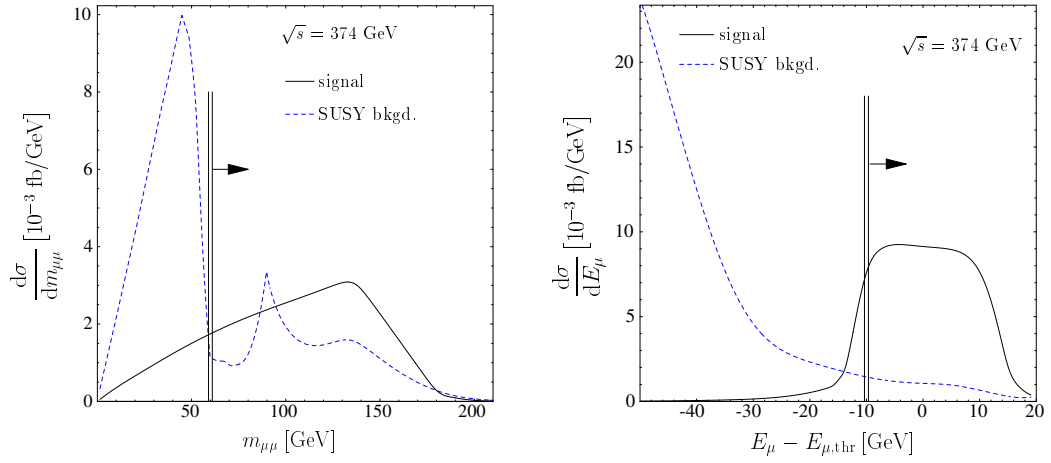which amounts to 60 GeV for the mass values of the reference point. In addition, requiring

(a)
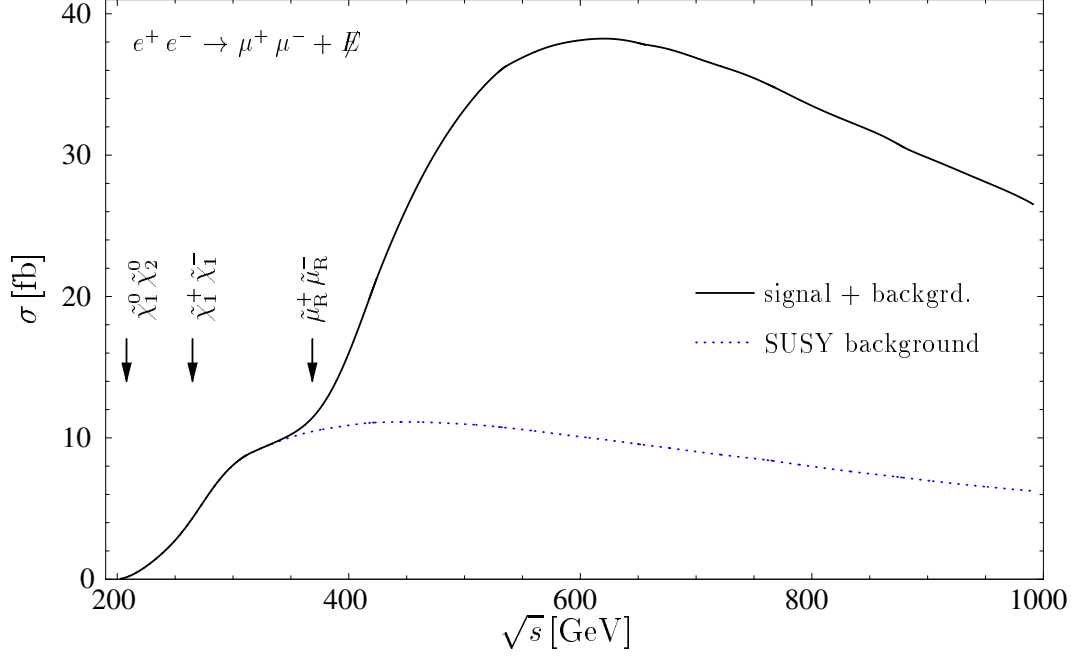
(b)

Figure 4: (a) The total cross-section and SUSY backgrounds to $e^+e^- \rightarrow \mu^+\mu^- + \not{E}$, indicating the important nominal thresholds by arrows. (b) The distributions in the muon-pair invariant mass (after the missing energy cut has been made) and in the muon energy, with possible cuts shown as a double vertical line.

Source Process	Followed by	
$e^+e^- \to \tilde{\chi}_k^0 \tilde{\chi}_1^0$	$\tilde{\chi}_k^0 \to \mu^+\mu^-\tilde{\chi}_1^0$	
$e^+e^- \to \tilde{\chi}_2^0 \tilde{\chi}_2^0$	$\tilde{\chi}_2^0 \to \mu^+\mu^-\tilde{\chi}_1^0$	$\tilde{\chi}_2^0 \to \bar{\nu}\nu\tilde{\chi}_1^0$
$e^+e^- \to \tilde{\chi}_1^+ \tilde{\chi}_1^-$	$\tilde{\chi}_1^\pm \to \mu^\pm\nu_\mu\tilde{\chi}_1^0$	
$e^+e^- \to ZZ$	$Z \to \mu^+\mu^-$	$Z \to \tilde{\chi}_1^0\tilde{\chi}_1^0$
$e^+e^- \to Z\,h_0/H_0$	$Z \to \mu^+\mu^-$	$h_0/H_0 \to \tilde{\chi}_1^0\tilde{\chi}_1^0$

Table 1: *The significant doubly-resonant SUSY background processes contributing to* $e^+e^- \to \mu^+\mu^- + \not{\!E}$ *near the* $\tilde{\mu}_R^+\tilde{\mu}_R^-$ *production threshold. Singly-resonant and non-resonant SUSY backgrounds are also included in the analysis.*

the missing energy $\not{\!E}$ below the cut

$$\not{\!E} \lesssim E_{\text{cut}} = \sqrt{s}\left[1 - \frac{(m_{\tilde{\chi}_2^0}^2 - m_{\tilde{\chi}_1^0}^2)\left(s - m_{\tilde{\chi}_1^0}^2 + m_{\tilde{\chi}_2^0}^2 - \lambda^{1/2}(s, m_{\tilde{\chi}_1^0}^2, m_{\tilde{\chi}_2^0}^2)\right)}{4\,m_{\tilde{\chi}_2^0}^2\,s}\right] \quad (20)$$

eliminates a large fraction of the background events from $\tilde{\chi}_1^0\tilde{\chi}_2^0$ cascades to $\mu^+\mu^-\tilde{\chi}_1^0\tilde{\chi}_1^0$. In the scenario *RR2* , events with missing energy below a fraction 0.63 of the c.m. energy are kept in the signal sample. Only a small number of signal events are lost while the $\tilde{\chi}_1^0\tilde{\chi}_2^0$ background is reduced by a factor of fifty. After applying these two cuts we are left with a small amount of higher cascade decays. This is apparent from Fig. 4(b/left) which shows the invariant μ-pair mass after the missing energy cut has already been applied.

Near the threshold the observed muon energy is sharp:

$$E_\mu \approx (m_{\tilde{\mu}}^2 - m_{\tilde{\chi}_1^0}^2)/2m_{\tilde{\mu}} \quad (21)$$

Alternatively to the $\not{\!E}$ cut, the signal to background ratio can also be greatly enhanced by selecting muons with energies in a band $\Delta E \approx 10$ GeV about the nominal threshold energies, cf. Fig. 4(b/right).

The matrix elements are calculated using the computer algebra package *FeynArts* [12]. Due to the large number of diagrams involved, i.e. more than 300, it is convenient to perform the evaluation in terms of helicity amplitudes which are then evaluated using the Dirac spinor techniques of Ref. [13]. The phase-space integration can be performed by multi-channel Monte-Carlo methods where appropriate phase-space mappings may be used in order to obtain numerically stable results of high accuracy [14]. The Monte-Carlo
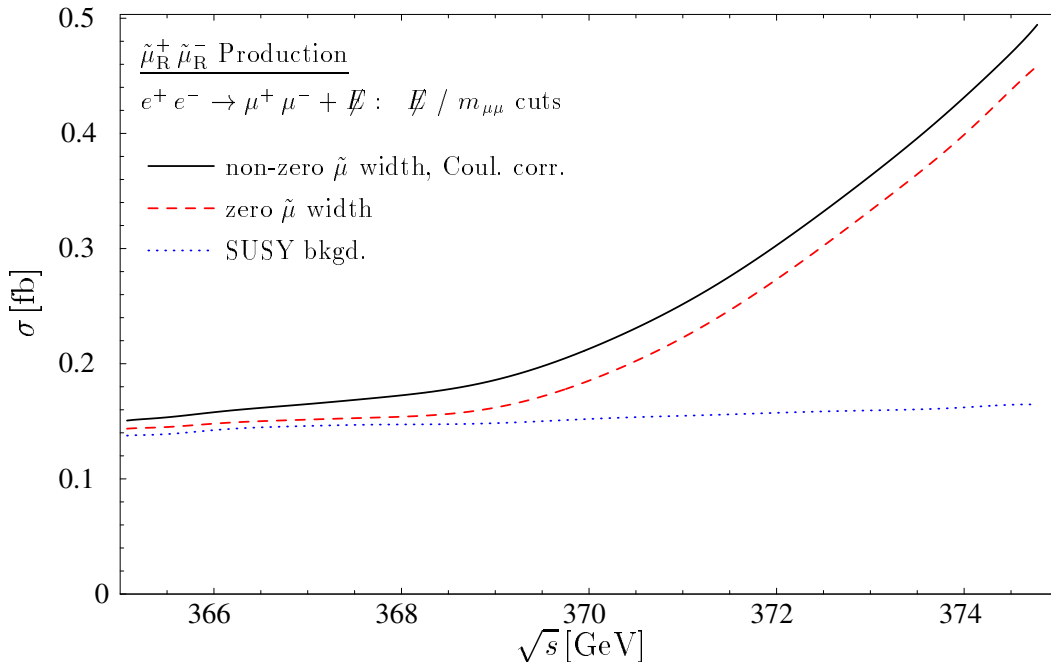
9

Figure 5: *The excitation curves for the signal (with non-zero width and Coulomb rescattering, compared with zero width) and the SUSY background after the missing energy cut.*

error is reduced by adaptive weight optimization [15]. Initial state radiation from emission of collinear and soft photons is included using the structure-function method [16] up to second order in the leading-log approximation and soft-photon exponentiation [17]. Beamstrahlung effects are also included using the program $K\iota\rho\kappa\eta$ [18] for TESLA accelerator design parameters.

2.3   Results

Including the SUSY backgrounds, the excitation curves, after the beamstrahlung is switched on and the cuts are applied, are shown in Fig. 5 for the missing-energy cut as a characteristic example (similar results follow from the muon-energy cut). As evident from the figure, the background is smooth below the signal curve in the threshold region. The background can therefore be extrapolated from below into the threshold region and subtracted experimentally in a model-independent way since interference effects are small.

3 Selectron Excitation

3.1 Diagonal Selectron Pairs in $e^- e^-$ Collisions

Among the S-wave production processes for left- and right-chiral selectrons, the $e^- e^-$ collisions are of particular interest. Even though mixed pairs in $e^+ e^-$ collisions are also produced in S-waves, large SM and SUSY backgrounds (in particular production of neutralino and chargino pairs as listed in Tab.1 and heavier states followed by cascade decays) render these channels less attractive. The analysis will therefore be presented in detail for the channels $e^- e^- \to \tilde{e}_L^- \tilde{e}_L^-, \tilde{e}_R^- \tilde{e}_R^-$. The degree of polarization for the electron beams will be assumed 80%. In between the $\tilde{e}_R^- \tilde{e}_R^-$ and $\tilde{e}_L^- \tilde{e}_L^-$ thresholds, the impurity of the electron helicity states will also generate mixed $\tilde{e}_L^- \tilde{e}_R^-$ events which however are P-wave suppressed.

Pairs of <u>right-chiral selectrons $\tilde{e}_R^-$</u> almost completely decay into the final state $e^- e^- \tilde{\chi}_1^0 \tilde{\chi}_1^0$, resulting in the experimental signature of two electrons plus missing energy. The SM backgrounds predominantly arise from single W and Z production and can be reduced with the help of beam polarization and cutting on invisibly decaying Z bosons [19]. These cuts have little impact on the signal. This study therefore focuses on the supersymmetric backgrounds, which had not been included before. The relevant SUSY backgrounds with the signature $e^- e^- + \not{E}$ do not contain any pair production processes and turn out to be small over the full energy scale under consideration.

Pairs of <u>left-chiral selectrons $\tilde{e}_L^-$</u> can be selected by choosing a unique final state. If
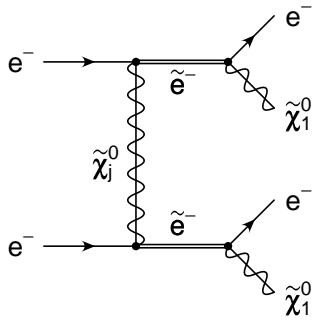
(a) <u>$e^- e^- \to e^- e^- \tilde{\chi}_1^0 \tilde{\chi}_1^0$</u>   (b) <u>$e^- e^- \to \nu_e \nu_e \tilde{\chi}_1^- \tilde{\chi}_1^-$</u>
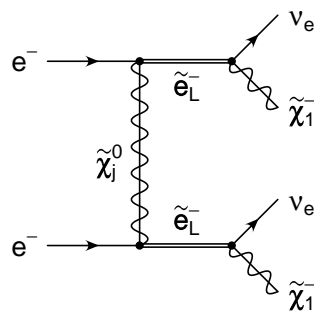

Figure 6: *The doubly resonant contributions to the processes (a) $e^- e^- \to e^- e^- \tilde{\chi}_1^0 \tilde{\chi}_1^0$ and (b) $e^- e^- \to \nu_e \nu_e \tilde{\chi}_1^- \tilde{\chi}_1^-$.*
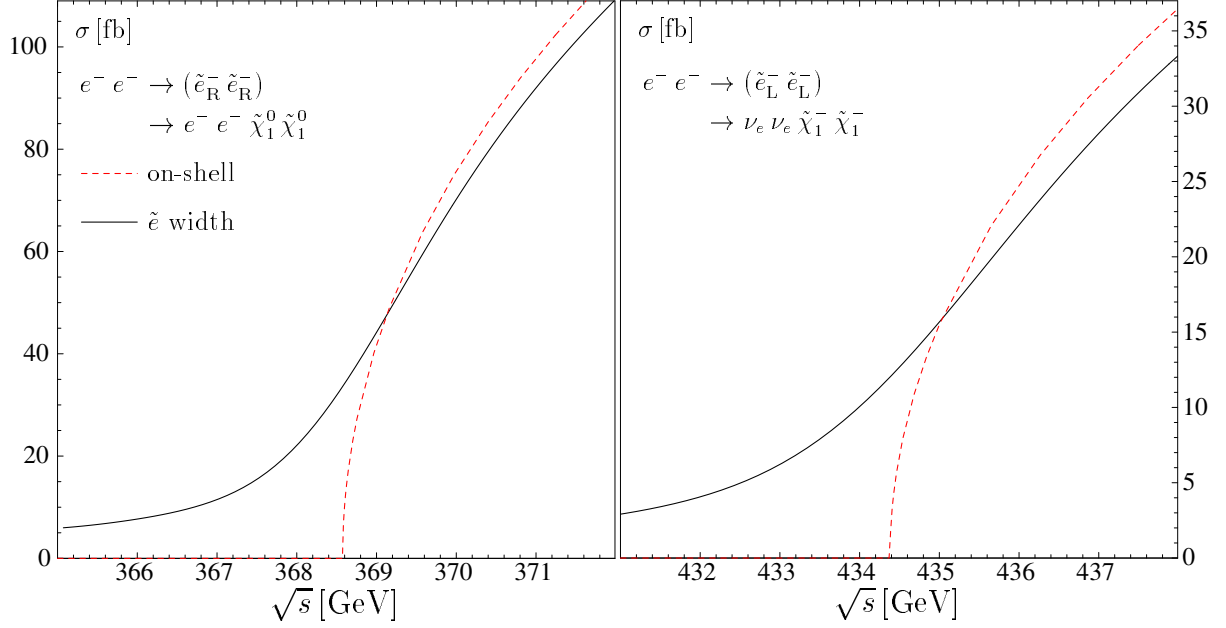
Figure 7: *The effect of finite selectron widths on the $e^- e^- \to \tilde{e}_R^- \tilde{e}_R^- \to e^- e^- \tilde{\chi}_1^0 \tilde{\chi}_1^0$ and $e^- e^- \to \tilde{e}_L^- \tilde{e}_L^- \to \nu_e \nu_e \tilde{\chi}_1^- \tilde{\chi}_1^-$ cross-sections.*

kinematically accessible, the main decay channel is the decay into charginos, $\tilde{e}_L^- \to \nu_e \tilde{\chi}_k^-$, eq. (11), with a branching ratio of more than 50%. It is convenient to consider a leptonic decay channel of one of the charginos, $\tilde{\chi}_1^- \to l^- \bar{\nu}_l \tilde{\chi}_1^0$ with $l \neq e$, and a hadronic decay channel of the second chargino, $\tilde{\chi}_1^- \to q \bar{q}' \tilde{\chi}_1^0$. About 30% of the chargino pairs follow these combined decay modes. The resulting signature $l q \bar{q}' + \not{E}$ is contaminated by only little SUSY backgrounds[4].

3.2   Results

The threshold cross-sections for $e_R^- e_R^- \to \tilde{e}_R^- \tilde{e}_R^-$ and $e_L^- e_L^- \to \tilde{e}_L^- \tilde{e}_L^-$ are shown in Fig. 7 for zero and non-zero width, respectively.

Since the amplitudes corresponding to the diagrams in Fig. 6 do not include any gauge boson exchanges, no specific attention needs to be paid to gauge invariance. These cross-sections, including the non-zero width, may therefore be interpreted as "signal cross-sections". However, for a systematic analysis, it is necessary to include all contributions with the four fermion final states. Coulombic photon rescattering effects are described

---

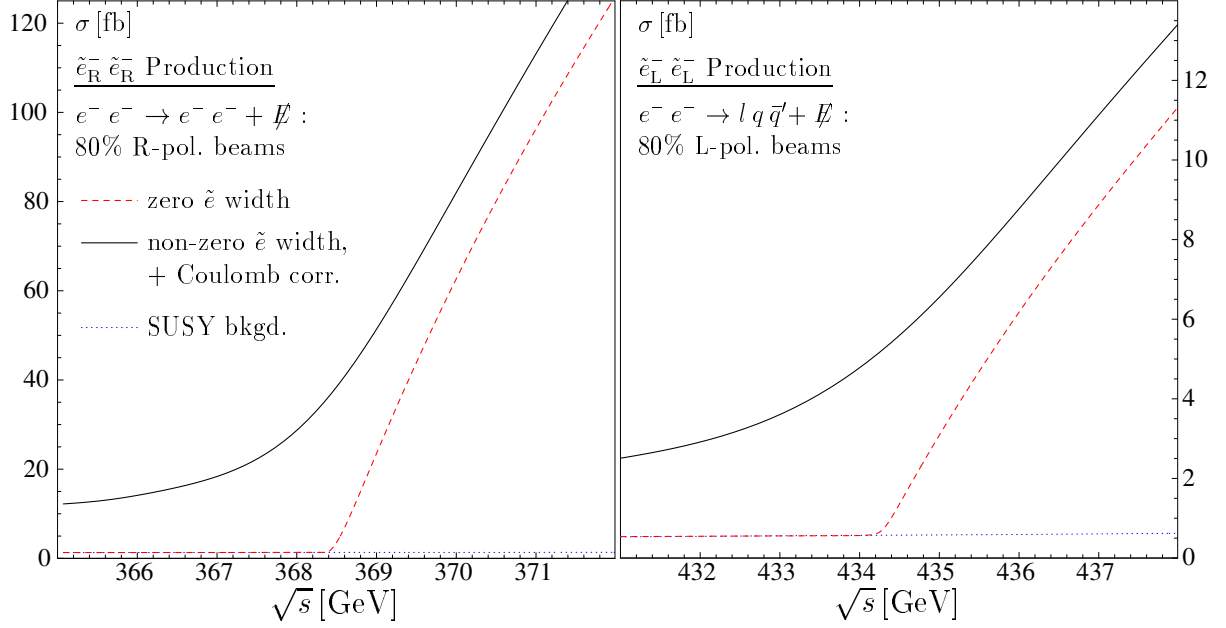[4]The SM backgrounds are kept small by this choice, too.

Figure 8: *The excitation curves for the signal (with non-zero width and Coulomb rescattering, compared with zero width) and the SUSY background near the $\tilde{e}_R\tilde{e}_R$ and $\tilde{e}_L\tilde{e}_L$ thresholds.*

by the modified Sommerfeld correction with $\mathcal{C}_0 = 1$ in eq. (15).

The final results are presented in Fig. 8. The figures prove that contributions from SUSY backgrounds are small and do not require additional cuts. They exhibit a flat energy dependence, thereby easily allowing their experimental subtraction from the excitation curves. The effect of Coulomb rescattering is more pronounced for S-wave threshold production in contrast to the P-wave smuon case.

4   Summary

The present report describes a first theoretical step into the area of high-precision analyses in supersymmetric theories. We have concentrated on non-zero width and Coulomb rescattering effects in the threshold production of smuon and selectron pairs. Moreover, SUSY backgrounds to SUSY signals are systematically analyzed.

For smuon pair production, $e^+e^- \to \tilde{\mu}_R^+\tilde{\mu}_R^-, \tilde{\mu}_L^+\tilde{\mu}_L^-$, proper attention must be paid to the gauge invariance of the amplitudes when non-zero widths are included. These effects are of the same size as the expected experimental resolution. In contrast to P-wave smuon

13

production, which is $\propto \beta^3$ near threshold, selectron pairs can be generated in S-waves with a steep rise $\propto \beta$ of the threshold cross-section. This advantage can be exploited in e^+e^- and e^-e^- collisions. However, SUSY and SM backgrounds in e^-e^- collisions are significantly smaller, so that $e_R^- e_R^- \rightarrow \tilde{e}_R^- \tilde{e}_R^-$ and $e_L^- e_L^- \rightarrow \tilde{e}_L^- \tilde{e}_L^-$ are the preferred production processes for right- and left-chiral selectrons $\tilde{e}_R$ and $\tilde{e}_L$.

It is evident that many additional detailed calculations of genuine higher order effects must follow to reach final theoretical accuracies at a level of a per-mille as required by the expected accuracy of e^+e^- linear colliders.

Note: Shortly before completing the manuscript we learned about a similar analysis of non-zero width effects in the threshold production of right-chiral selectrons at electron colliders by J. L. Feng and M. E. Peskin [hep-ph/0105100].

Acknowledgments

Appendix

Reference scenario $RR2$ with $\tan\beta = 30$ $(l = e, \mu)$:

Neutralino masses:

	$m_{\tilde{\chi}_i^0}$ [GeV]
$\tilde{\chi}_1^0$	74.81
$\tilde{\chi}_2^0$	133.04
$\tilde{\chi}_3^0$	272.81
$\tilde{\chi}_4^0$	292.96

Chargino masses:

	$m_{\tilde{\chi}_i^\pm}$ [GeV]
$\tilde{\chi}_1^\pm$	132.35
$\tilde{\chi}_2^\pm$	294.84

Right-chiral slepton $\tilde{l}_R$:

Mass $m_{\tilde{l}}$	184.29 GeV
Width $\Gamma_{\tilde{l}}$	0.62 GeV

Branching Ratios	
$\tilde{l}_R^- \to l^- \tilde{\chi}_1^0$	0.991
$\to l^- \tilde{\chi}_2^0$	0.008
$\to l^- \tilde{\chi}_{3,4}^0$	—

Left-chiral slepton $\tilde{l}_L$:

Mass $m_{\tilde{l}}$	217.19 GeV
Width $\Gamma_{\tilde{l}}$	1.03 GeV

Branching Ratios	
$\tilde{l}_L^- \to l^- \tilde{\chi}_1^0$	0.144
$\to l^- \tilde{\chi}_2^0$	0.338
$\to l^- \tilde{\chi}_{3,4}^0$	—
$\to \nu_l \tilde{\chi}_1^-$	0.517
$\to \nu_l \tilde{\chi}_2^-$	—

References

[1] J. Wess and B. Zumino, Nucl. Phys. B **70** (1974) 39; Phys. Lett. B **49** (1974) 52.

[2] E. Accomando et al, Phys. Rept. **299** (1998) 1.

[3] H. U. Martyn and G. A. Blair, Proceedings, *4th International Workshop on Linear Colliders* (LCWS 99), Sitges 1999, [hep-ph/9910416]; H. U. Martyn, Workshop on Physics at TeV Colliders, Les Houches 1999, [hep-ph/0002290] and in *Conceptual Design of a 500 GeV e^+e^- Linear Collider*, eds. R. Brinkmann et al., DESY 1997-048 and ECFA 1997-182.

[4] G. A. Blair, W. Porod and P. M. Zerwas, Phys. Rev. D **63** (2001) 017703.

[5] M. K. Gaillard, L. Hall and I. Hinchliffe, Phys. Lett. B **116** (1982) 279; M. Glück and E. Reya, Phys. Lett. B **130** (1983) 423; R. M. Barnett, H. E. Haber and K. S. Lack-

ner, Phys. Rev. D **29** (1984) 1381; D. H. Schiller and D. Wahner, Nucl. Phys. B **255** (1985) 505; T. Kobayashi and M. Kuroda, Phys. Lett. B **134** (1984) 271;

[6] W. Y. Keung and L. Littenberg, Phys. Rev. D **28** (1983) 1067; C. A. Heusch (ed.), Proceedings, *International Workshop on Electron-Electron Interactions at TeV Energies* (e^-e^- 95/97/99), Santa Cruz 1995, 1997, 1999, Int. J. Mod. Phys. A **11** (1996) 1523; *ibid.* A **13** (1998) 2217; *ibid.* A **15** (2000) 2347; J. L. Feng, Int. J. Mod. Phys. A **13** (1998) 2319.

[7] T. Schimert and X. Tata, Phys. Rev. D **32** (1985) 721; A. Bartl, H. Fraas and W. Majerotto, Z. Phys. C **34** (1987) 411; T. Tsukamoto, K. Fujii, H. Murayama, M. Yamaguchi and Y. Okada, Phys. Rev. D **51** (1995) 3153; B. de Carlos and M. A. Diaz, Phys. Lett. B **417** (1998) 72.

[8] See *e.g.*, V. S. Fadin, V. A. Khoze, A. D. Martin and A. Chapovsky, Phys. Rev. D **52** (1995) 1377; A. Denner, S. Dittmaier, M. Roth and D. Wackeroth, Nucl. Phys. B **560** (1999) 33.

[9] TESLA Technical Design Report, Part III, eds. R. Heuer, D. J. Miller, F. Richard and P. M. Zerwas, DESY-2001-11C; S. Ambrosanio, G. A. Blair and P. M. Zerwas, *A Study of* SUGRA *for the Linear Collider*, [http://www.hep.ph.rhbnc.ac.uk/~blair/susy].

[10] A. Sommerfeld, *Atombau und Spektrallinien*, Bd. 2, (Vieweg, Braunschweig 1939); A. D. Sakharov, JETP **18** (1948) 631.

[11] V. S. Fadin and V. A. Khoze, JETP Lett. **46** (1987) 525; Sov. J. Nucl. Phys. **48** (1988) 309 and *Proc. of the 24th LNPI Winter School*, Leningrad (1989), vol. 1, p.3.

[12] J. Küblbeck, M. Böhm, A. Denner, Comput. Phys. Commun. **60** (1991) 165; A. Denner, H. Eck, O. Hahn and J. Küblbeck, Nucl. Phys. B **387** (1992) 467; T. Hahn, hep-ph/0012260; T. Hahn, *FeynArts 3 User's Guide*, [http://www.feynarts.de/]; T. Hahn and C. Schappacher, hep-ph/0105349.

[13] R. Kleiss and W. J. Stirling, Nucl. Phys. B **262** (1985) 235.

[14] F. A. Berends, P. H. Daverveldt and R. Kleiss, Nucl. Phys. B **253** (1985) 441 and Comput. Phys. Commun. **40** (1986) 285; J. Hilgart, R. Kleiss and F. Le Diberder,

Comput. Phys. Commun. **75** (1993) 191; F. A. Berends, R. Pittau and R. Kleiss, Nucl. Phys. B **424** (1994) 308.

[15] R. Kleiss and R. Pittau, Comput. Phys. Commun. **83** (1994) 141.

[16] E. A. Kuraev and V. S. Fadin, Sov. J. Nucl. Phys. **41** (1985) 466; G. Altarelli and G. Martinelli, in *Physics at LEP*, eds. J. Ellis and R. Peccei, CERN-86-02.

[17] D. R. Yennie, S. C. Frautschi and H. Suura, Annals Phys. **13** (1961) 379; F. A. Berends *et al*, in *Z Physics at LEP 1*, eds. G. Altarelli, R. Kleiss and C. Verzegnassi, CERN-89-08.

[18] T. Ohl, Comput. Phys. Commun. **101** (1997) 269.

[19] F. Cuypers, G. J. van Oldenborgh and R. Rückl, Nucl. Phys. B **409** (1993) 128.